PROCEEDINGS, 50th Workshop on Geothermal Reservoir Engineering
Stanford University, Stanford, California, February 10-12, 2025
SGP-TR-229

Water-Based Geothermal Binary Cycles

Daniel W. Dichter

501 Massachusetts Avenue, Cambridge MA 02139

daniel.dichter@quaise.energy

Keywords: water, binary, cycle, utilization, efficiency, superhot rock, SHR, organic Rankine cycle, ORC, optimization, working fluid, heat exchanger, steam, turbine, exergy, stage, blade, LSB

ABSTRACT

A water-based geothermal binary cycle may be defined as a power cycle in which geofluid transfers heat to pure water in a non-mixing heat exchanger, producing clean steam suitable for a turbine-generator. This work shows that these cycles are an attractive alternative to organic Rankine cycles (or ORCs) for geothermal resources producing at around 300-350 °C, especially if geofluid characteristics preclude a dry steam or flash cycle. It is known in both theoretical and practical terms that higher resource temperatures entail improvements in thermal efficiency, utilization (or exergetic efficiency), and power output. At currently accessible temperatures, typically 100-250 °C, the preferred type of binary cycle is an ORC, which uses a liquid hydrocarbon as its working fluid. An example is given of how to define a typical ORC and determine its optimal design parameters, using a gradient ascent algorithm with the criterion of maximizing utilization. Curve matching by pinch point equalization within the heat exchanger is noted as an emergent feature of optimized cycles in temperature-heat transfer (or T-q) coordinates. Special attention is given to the sizing of the turbine, in the sense of its number of stages and last-stage blade length. This methodology is then generalized to multi-stage (i.e. multi-pressure) and superheated cycles, with wider ranges of production temperatures and working fluids. It is shown that water outperforms most ORC hydrocarbons except cyclopentane for production temperatures above about 300 °C, and is preferable in terms of cost, safety, and scalability. The performance of these water-based binary cycles is then compared in greater detail against cyclopentane ORCs for a variety of production scenarios at 350 °C, including saturated liquid, saturated vapor, and superheated vapor. Water was found to confer more flexibility in cycle design because of its higher critical temperature and non-retrograde condensation, yielding superior thermal efficiency and utilization, ranging from about 22-27% and 61-75% respectively. It was also found that although ORCs entail a somewhat more compact turbine, water seems to confer more significant advantages relating to the costs of the wells, heat exchanger, and condenser.

1. INTRODUCTION

1.1 History of Geothermal Power Cycles

The first commercial geothermal power plant, Larderello 1, began operating in Italy in 1914 with a water-based binary cycle, also known as an “indirect” cycle (DiPippo, 2016, p. 330). This choice of cycle was motivated by the corrosivity of the geofluid, which was incompatible with contemporary turbomachinery, and by the limited availability of non-aqueous fluids and their thermal-physical properties (Macchi and Astolfi, 2017, p. 31). By the 1950s and 1960s, sufficient progress had been made in turbomachinery design that “direct” cycle plants became practical, using dry steam and flash cycles, i.e. without a vaporizing heat exchanger. Concurrently, the organic Rankine cycle (ORC) was conceptualized and demonstrated at small scales, restarting the development of binary plants (Tabor and Bronicki, 1962). This culminated in the commissioning of the first modern ORC geothermal plants in the 1970s and 1980s. The last of the water-based binary plants at Larderello was converted to a direct dry steam cycle in 1968, and the later proliferation of ORCs led to the terms “binary” and “ORC” becoming interchangeable. The contemporary geothermal landscape now consists of dry steam cycles, flash cycles, and ORCs, with plants often incorporating multiple stages and/or combined cycles to improve performance. Binary cycles are increasingly chosen over direct-use cycles, especially flash, for their superior ability to utilize low-temperature and/or highly contaminated geofluid (DiPippo, 2016, p. 195).

1.2 Analog of Nuclear Fission Power Plants

Although water-based binary cycles were phased out of geothermal power, they are nonetheless common in nuclear power generation, in the form of the pressurized water reactor, or PWR. Power plants of this type have been operating since the 1950s (Li and Priddy, 1982, p. 188). In this type of plant, the reactor core is continuously cooled with “light” or normal water kept at a sufficiently high pressure that it remains in the liquid phase, typically exiting the reactor core at around 300 °C and 150 bar. In a non-mixing heat exchanger called a steam generator, the coolant then transfers heat to a lower-pressure working fluid of pure water almost isothermally, producing saturated to slightly superheated vapor, sometimes with reheating. This vapor is supplied to a turbine and expanded, producing work and electricity, then condensed and recirculated as in a Rankine cycle. Although PWRs are not usually referred to as binary cycles, they nonetheless meet the basic criterion of using two separate fluids for heat and work transfer with a non-mixing heat exchanger.

1.3 Significance of Source Temperature

The maximum thermal efficiency achievable by a heat engine is Carnot efficiency $\eta_{I,Carnot}$ (Çengel et al., 2012, p. 355). Achieving Carnot efficiency requires that all heat transfers are both isothermal and reversible, which is not possible for real-world heat engines operating with finite time and mass. Accordingly, later researchers proposed more realistic definitions of ideal thermal efficiency, which are necessarily less than Carnot efficiency. DiPippo noted that in binary cycles, geofluid produced in the liquid phase declines linearly in temperature as it heats and vaporizes the working fluid, and a so-called "triangular" cycle may be defined between the temperature limits (DiPippo, 2016, p. 208). More generally, it was also observed by Curzon and Ahlborn (1975), and originally by Reitlinger (1927), that heat engines are usually operated at or near their maximum power output, which is equivalent to operating with maximum utilization or exergetic efficiency, as described in Section 3.1. For each of these idealized cases, it was shown that thermal efficiency depends solely on the heat engine's temperature limits, as follows:

$$\eta_{I,Carnot} = 1 - \frac{T_c}{T_h} \quad (1)$$

$$\eta_{I,triangular} = \frac{T_h - T_c}{T_h + T_c} \quad (2)$$

$$\eta_{I,Reitlinger} = 1 - \sqrt{\frac{T_c}{T_h}} \quad (3)$$

Where T_c and T_h refer to the "cold" and "hot" (or source) temperatures, calculated in Kelvin. These are plotted in Figure 1 below for $T_c = 50$ °C. This choice of T_c is further discussed in Section 3.2.

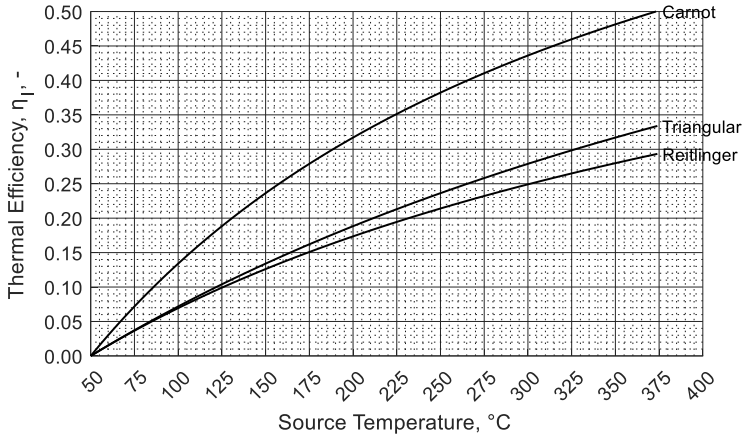

Figure 1: Ideal heat engine thermal efficiencies as functions of source temperature.

These relations show that the performance of a heat engine improves significantly as its source temperature increases. Further, a heat engine's source temperature is also a primary factor in determining the most appropriate choice of working fluid. Systemization of power cycles according to their source temperatures shows approximate ranges of 100-300 °C for ORCs, 200-600 °C for steam cycles, and 600-1,500 °C for gas (i.e. Brayton) cycles (Macchi and Astolfi, 2017, p. 300). This concept is discussed further in Section 5.

2. PLANT MODEL

This section provides methodology for defining an ideal binary cycle and determining its performance, given a certain geofluid production scenario – for example, temperature T_a, enthalpy h_a, and mass flow rate $\dot{m}_g$. A double-pressure saturated cycle is described as an example. Single- and triple-pressure cycles, as well as superheated cycles, can similarly be analyzed by adapting this methodology.

2.1 Working Fluid

A plant schematic and a T-s (temperature-entropy) diagram are shown in Figures 2 and 3 below. This model is characterized by isobaric heat transfers (3-2, 8-7, 10-9), isentropic pumping (9-8, 4-3), and a non-isentropic turbine (2-5, 6-10). The working fluid cycle may be defined by the working fluid composition (e.g. butane, pentane, water, etc.), the saturation temperatures T_1, T_4, and T_9, and either mass flow rate fraction, m_{LP} or m_{HP}, where the subscripts refer to the low-pressure and high-pressure portions of the cycle, such that $m_{LP} + m_{HP} = 1$. Note for example that $m_{LP} = m_7$, $m_{HP} = m_2$, and $m_9 = 1$. Additional parameters related to the heat exchanger, turbine, and condenser are discussed in Section 3.2.

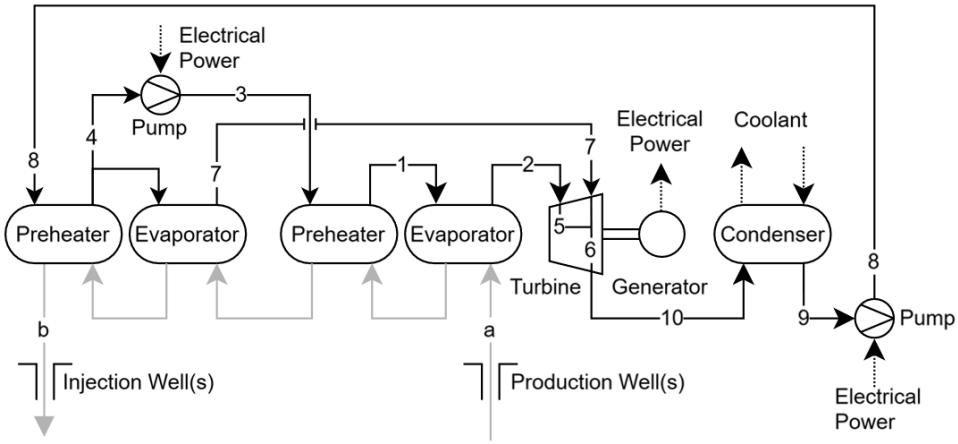

Figure 2: Schematic of a double-pressure saturated binary plant. Black arrows denote working fluid; gray denotes geofluid.

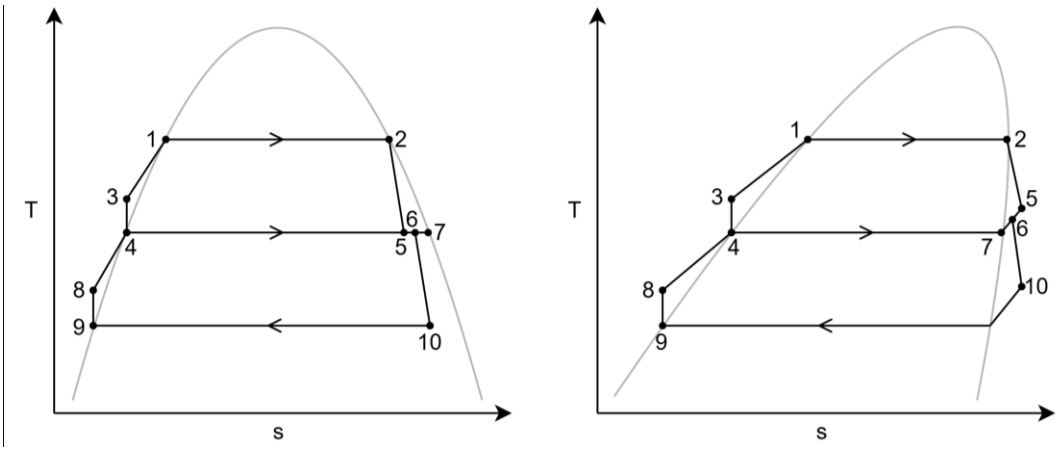

Figure 3: Temperature-entropy (T-s) diagrams of saturated double-pressure binary cycles for non-retrograde (left) and retrograde (right) fluids, not to scale.[1] State points are labeled from top to bottom, left to right, with respect to a non-retrograde fluid. Gray lines denote phase boundaries.

The working fluid exits the condenser (10-9) as a saturated liquid slightly above the ambient temperature in a dead state. It is then pumped isentropically (9-8) to the saturation pressure P_4 corresponding to temperature T_4. The low-pressure preheater (8-4) then isobarically heats the working fluid, producing saturated liquid. This then branches into two parallel paths: high-pressure, and low-pressure.

Most of the working fluid flows through the high-pressure path, where it is again pumped isentropically (4-3) to the saturation pressure P_1 corresponding to temperature T_1. It is then preheated isobarically (3-1) to saturated liquid, and vaporized isobarically (1-2), yielding saturated vapor. This vapor is then partially expanded (2-5) in the turbine to pressure P_5 with dry isentropic efficiency η_t, producing a work output. The Baumann rule is accounted for with non-retrograde fluids such as water, which are characterized by $x_5 < 1$ (DiPippo, 2016, p. 122). Meanwhile, the low-pressure working fluid is isobarically vaporized in the low-pressure evaporator (4-7), producing saturated vapor.

The fluid streams at States 5 and 7 are of equal pressure, allowing them to be mixed (5-6, 7-6). This may be either internal to the turbine, with dual admission as depicted in Figure 2, or external to it, with separate LP and HP turbines. In either case, this mixing process is

[1] Retrograde refers to the quantity $\partial T / \partial s$ evaluated at the saturated vapor boundary. Where negative such as with water, expansion causes partial condensation; where positive as with hydrocarbons, expansion causes superheating. This is discussed further in Sections 4 and 6.

ideally adiabatic and isobaric, so conservation of energy dictates that $h_6 = h_5\, m_5 + h_7\, m_7$, where h denotes specific enthalpy. This mixed vapor is then expanded to the condenser pressure P_9 in the turbine (6-10), again with dry isentropic efficiency η_t and the Baumann rule if $x_{10} < 1$, producing an additional work output. Heat is then rejected from the working fluid isobarically (10-9), producing saturated liquid, and completing the cycle.

The heat output of the cycle is given by:

$$q_{out} = h_{10} - h_9 \tag{4}$$

The heat input must account for the branched flow, as follows:

$$q_{in} = (h_4 - h_8) + (h_7 - h_4)\, m_7 + (h_2 - h_3)\, m_2 \tag{5}$$

The net work w_{net} and thermal efficiency η_I can then be calculated conventionally (Çengel et al., 2012, p. 380):

$$w_{net} = q_{in} - q_{out} \tag{6}$$

$$\eta_I = 1 - \frac{q_{out}}{q_{in}} = \frac{w_{net}}{q_{in}} \tag{7}$$

Finally, a T-q (or temperature-heat transfer) curve is calculated by joining a series of curve segments in order of increasing temperature, with one segment per heat addition process (DiPippo, 2016, p. 200). Each segment's individual dimension in q is proportional to the product of its mass flow rate fraction m and enthalpy difference Δh, and the segments are scaled such that their overall dimension in q is equal to one, or 100%. The temperature along the T-q curve is determined by pressure-enthalpy lookup, using the pressure corresponding to each segment, and interpolating linearly between the enthalpy values at the segment boundaries. The resulting T-q curve is required to determine the geofluid outlet temperature, and the working fluid mass flow rate, as described in the following section.

2.2 Heat Exchanger

It is helpful to consider the discrete preheaters and evaporators collectively as a single heat exchanger acting on the two fluids.[2] At all points throughout the heat exchanger, the geofluid must maintain a sufficiently large temperature difference ΔT with respect to the working fluid, so that heat transfers in the intended direction and at a practical rate. Any point where the temperature difference between the two fluids is at a local minimum is referred to as a pinch point (DiPippo, 2016, p. 201). These often occur between preheaters and evaporators, as shown in Sections 4 and 6. A pinch point temperature difference of $\Delta T_{pp} = 10$ °C is assumed based on typical values (DiPippo, 2016, p. 218). This temperature difference causes an irreversibility, or loss, that is characteristic of heat exchangers, similar to the flash-separation process in a flash plant. Strategies for minimizing this loss using the concept of exergy are discussed throughout the remainder of this paper.

As a result, the geofluid outlet temperature T_b must be bounded by the geofluid production temperature T_a and the condenser temperature T_9; that is, $T_9 < T_b \leq T_a$. However, in cases of two-phase or vaporous geofluid production with $0 < x_a \leq 1$, heat transfer from the geofluid is not fully sensible as temperature because of isothermal condensation, i.e. a phase change. Therefore, it is more robust to state that the geofluid outlet entropy s_b must attain an intermediate value between the production entropy s_a and a dead state entropy s_o corresponding to saturated liquid at the working fluid's condenser temperature T_9; that is, $s_o < s_b < s_a$.

Using these limits, the working fluid's T-q curve, and the specified value of ΔT_{pp}, the geofluid outlet entropy s_b can be determined numerically with arbitrary precision using the bisection method. Each iteration requires calculating a geofluid T-q curve by adapting the method described in Section 2.1, assessing how the minimum temperature difference between the two curves compares to the specified value of ΔT_{pp}, and adjusting the entropy limits for s_b accordingly. Once the geofluid outlet entropy s_b is determined, the remaining properties T_b and h_b can be obtained by lookup, since ideally $P_b = P_a$.

The heat exchanger is ideally sufficiently well-insulated that it can be treated as adiabatic. Thereby, the heat transfer rate from the geofluid is ideally equal and opposite to the heat transfer rate to the working fluid, per conservation of energy. Accordingly, the mass flow rate of the working fluid $\dot{m}_w$ can be determined:

$$\Delta h_g\, \dot{m}_g + \Delta h_w\, \dot{m}_w = 0 \tag{8}$$

$$(h_b - h_a)\, \dot{m}_g + q_{in}\, \dot{m}_w = 0 \tag{9}$$

$$\dot{m}_w = \frac{(h_a - h_b)\, \dot{m}_g}{q_{in}} \tag{10}$$

Note that in general $\dot{m}_g \neq \dot{m}_w$. The heat transfer rate between the two fluids can then be expressed as:

[2] The condenser is also a type of heat exchanger, but is not referred to as such herein to avoid confusion with the preheaters and evaporators.

$$\dot{Q}_h = \dot{m}_w \, q_{in} = \dot{m}_g \, (h_a - h_b) \tag{11}$$

2.3 Overall Performance

The gross power output of the plant can be expressed as:

$$\dot{Q}_g = \dot{m}_w \, w_{net} \tag{12}$$

Similarly, the heat rejection from the condenser is given by:

$$\dot{Q}_c = \dot{m}_w \, q_{out} \tag{13}$$

The thermal efficiency of the plant as a whole is given by:

$$\eta_I = \frac{\dot{Q}_g}{\dot{Q}_h} = \frac{\dot{m}_w \, w_{net}}{\dot{m}_g \, (h_a - h_b)} = \frac{(h_a - h_b) \, w_{net}}{q_{in} \, (h_a - h_b)} = \frac{w_{net}}{q_{in}} \tag{14}$$

Note that the expression for $\dot{m}_w / \dot{m}_g$ was substituted from Equation 10. That is, the thermal efficiency of the plant simplifies to the thermal efficiency of the cycle; the two quantities are ideally indistinguishable. The specific exergy of the produced geofluid is given by:

$$e_a = (h_a - h_o) - T_o(s_a - s_o) \tag{15}$$

Where the subscript o again denotes the dead state, taken as saturated liquid at the condenser temperature T_9, and T_o is expressed in Kelvin (DiPippo, 2016, p. 296). The exergetic power is then given by:

$$\dot{E} = \dot{m}_g \, e_a \tag{16}$$

The utilization, or exergetic efficiency, of the plant as a whole is given by:

$$\eta_{II} = \frac{\dot{Q}_g}{\dot{E}} \tag{17}$$

Lastly, the effectiveness or specific output is given by (DiPippo, 2016, p. 154):

$$w = \frac{\dot{Q}_g}{\dot{m}_g} \tag{18}$$

2.4 Turbine Sizing

A single-flow axial turbine is assumed. It is often noted that the choice of working fluid significantly affects the physical size, and thereby the approximate cost, of the turbine (DiPippo, 2016, p. 206; Milora and Tester, 1976, p. 74; Tabor and Bronicki, 1962). Two primary quantities to this effect are the turbine's last-stage blade (or LSB) length r_{blade}, and its overall number of stages n. Note that a turbine stage is not to be confused with a cycle stage; the two concepts are distinct.

For both steam and ORC turbines, the blade roots have a significant radial displacement r_{hub} from the turbine's central axis. This offset significantly increases the cross-sectional outlet flow area for a given last-stage blade length r_{blade}, or equivalently reduces the flow velocity, if all else is held equal. The fluid velocity at the turbine outlet v_{out} is estimated as a constant fraction M, or Mach number, of the local sonic velocity v_s (DiPippo, 2016, p. 206):

$$v_{out} = M \, v_s \tag{19}$$

The sonic velocity v_s is defined as follows:

$$v_s = \sqrt{\frac{\partial P}{\partial \rho}}_{s=\text{const.}} \tag{20}$$

This can be calculated using finite differences in both the two-phase and vapor regions for retrograde and non-retrograde fluids. For the sake of estimation, it is assumed that $r_{hub} \approx 0.250$ m [9.8 in] and $M \approx 0.75$ based on observed values; that is, the turbine outlet velocity is approximately transonic.[3] The required outlet flow area can then be determined by:

[3] Based on available parameters for the Sonoma plant at The Geysers, formerly SMUDGEO #1, with 25 inch last-stage blades, four exhaust ends, and 72 MWe gross output capacity (DiPippo, 2016, p. 359).

$$A_{out} = \frac{\dot{m}_w}{\rho_{out}\, v_{out}} \tag{21}$$

The last-stage blade length can then be calculated geometrically using the quadratic formula:

$$r_{blade} = \frac{-\pi\, r_{hub} + \sqrt{(\pi\, r_{hub})^2 + \pi\, A_{out}}}{\pi} \tag{22}$$

Geothermal steam turbines are characterized by $r_{blade} \leq$ 25-30 inches (DiPippo, 2016, p. 147); fossil-fired steam turbines are significantly larger, with $r_{blade} \approx$ 26-56 inches (Siemens Energy, 2021).

Most axial turbines experience significant fluid compressibility; exceptions include wind and hydroelectric turbines (Macchi and Astolfi, 2017, p. 300). For this reason, they generally consist of multiple stages that progressively expand the working fluid, collectively producing a work output. The isentropic efficiency of a single turbine stage approaches its maximum value of around 90% as the volumetric flow rate ratio $\dot{V}_{out}/\dot{V}_{in} = \dot{V}_r \to 1$ (Macchi and Astolfi, 2017, p. 307). However, achieving $\dot{V}_r \to 1$ is impractical for flows with significant compressibility, as this causes the number of stages $n \to \infty$. To balance this tradeoff, it is assumed that each stage has a constant volumetric flow rate ratio $\dot{V}_r \approx 2$; that is, each stage approximately doubles the volumetric flow rate of the working fluid, giving near-optimal performance with a practical number of stages. Since the mass flow rate $\dot{m}_w$ is constant across a single stage by conservation of mass, it follows that $\dot{m} = \dot{V}\, \rho$, where ρ denotes volumetric mass density. Therefore, a stage with $\dot{V}_r \approx 2$ must also have $\rho_r \approx 1/2$, or a density ratio of one-half. In other words, $\dot{V}$ increases exponentially in the direction of flow, while ρ decreases exponentially, and the turbine as a whole may be modeled as:

$$\dot{V}_r{}^n = \frac{\rho_{in}}{\rho_{out}} \tag{23}$$

Using the change of base formula, this can be solved for n:

$$n \approx \text{ceil}\left(\frac{\log\left(\frac{\rho_{in}}{\rho_{out}}\right)}{\log(V_r)}\right) \tag{24}$$

Where ceil() denotes the ceiling function, such that n is a whole number with $\dot{V}_r \leq 2$. Characteristic values are $n \approx$ 4-8 for geothermal steam turbines (DiPippo, 2016, p. 118, 539), $n \approx$ 9-10 for fossil-fired steam turbines (Siemens Energy, 2021), and $n \approx$ 3-7 for ORC turbines (Martinez, 2024; Ormat, 2024). All plants shown later in Section 4 and 6 are scaled to a constant gross power output of $\dot{Q}_g = 25$ MWe, to compare the turbines' stage quantity n and last-stage blade length r_{blade}. This is achieved by adjusting the geofluid production rate $\dot{m}_g$, which can be thought of as varying the quantity of wells that comprise the geothermal field.

3. CYCLE OPTIMIZATION

In Section 2, the values of the parameters that define the working fluid cycle were considered as independent parameters. Accordingly, this section provides a method for determining optimal values of these parameters.

3.1 Criteria

In general, power plants are not optimized for any single criterion, as they must balance competing tradeoffs of output, efficiency, cost, reliability, and so on. Nonetheless, single-criterion optimization is useful to approximate balanced designs, and to understand limiting behavior. As described in Section 2, common overall performance criteria include:

1. Thermal efficiency:
$$\eta_I = 1 - \frac{q_{out}}{q_{in}} = \frac{w_{net}}{q_{in}} \tag{25}$$
2. Utilization, or exergetic efficiency:
$$\eta_{II} = \frac{\dot{Q}_g}{\dot{E}} = \frac{\dot{m}_w\, w_{net}}{\dot{m}_g\, e_a} \tag{26}$$
3. Effectiveness, or specific output:
$$w = \frac{\dot{Q}_g}{\dot{m}_g} = \frac{\dot{m}_w\, w_{net}}{\dot{m}_g} \tag{27}$$
4. Gross power output:
$$\dot{Q}_g = \dot{m}_w\, w_{net} \tag{28}$$

If the geofluid production conditions are assumed to be fixed, i.e. $\dot{m}_g$ and e_a, Equations 25-28 show that only two unique optimization criteria exist: thermal efficiency η_I, and utilization η_{II}, since:

$$\eta_{II} \propto w \propto \dot{Q}_g = \dot{m}_w \, w_{net} \tag{29}$$

That is, optimizing for effectiveness or gross power output is equivalent to optimizing for utilization. As described in Section 1, the Reitlinger (or Curzon-Ahlborn) efficiency indicates that heat engines are generally operated near their maximum power outputs, itself equivalent to maximum utilization η_{II}, rather than at their maximum thermal efficiency η_I. Corroborating this, geothermal flash and binary power plants often incorporate multiple cycle stages, despite either a neutral or negative effect on η_I, to increase η_{II} (DiPippo, 2016, p. 212). It can be shown that a general consequence of optimizing a binary cycle for thermal efficiency η_I is deficient heat transfer in the heat exchanger, an excessive geofluid reinjection temperature, i.e. $T_b \gg 100$ °C, and ultimately a suboptimal power output $\dot{Q}_g$. This parallels the observation by Curzon and Ahlborn (1975) that a heat engine of maximum (i.e. Carnot) thermal efficiency must operate "infinitely slowly" and thereby paradoxically attains zero power output. Similarly, it can be shown that the thermal efficiency of a Brayton cycle ideally approaches Carnot efficiency as the pressure ratio increases, but simultaneously the power output approaches zero (Çengel et al., 2012, p. 370). For these reasons, η_{II} is taken as the optimization criterion herein.

3.2 Framework

It was shown in Section 2 that a plant's performance can be determined from the working fluid composition and the independent parameters $[T_1,\ T_4,\ T_9,\ m_{LP}]$, given a certain geofluid production scenario $[T_a,\ s_a,\ \dot{m}_g]$ and set of plant component constants $[\Delta T_{pp},\ \eta_t]$. Per Section 1.3, it is advantageous for the condenser temperature T_9 to be as low as possible, but it must also be higher than that of the ambient air or water used for cooling. A conservative and constant value of $T_9 = 50$ °C is used herein, such that the condenser retains a temperature difference ΔT of at least 10 °C with an ambient temperature as high as 40 °C [104 °F]. Therefore T_9 can be taken as a plant constant rather than an independent parameter to be optimized. Altogether, the optimization can be stated formally as:

Find cycle parameters:	$[T_1,\ T_4,\ m_{LP}]$
That maximize:	η_{II}
Given geofluid production:	$[T_a,\ s_a,\ \dot{m}_g]$
Plant constants:	$[T_9 = 50\ °C,\ \Delta T_{pp} = 10\ °C,\ \eta_t = 0.85]$
And constraints:	$[x_5,\ x_6,\ x_{10}] \geq 0.85$
	$P_4 \geq 1$ bar

As described in Section 2.1, the quality constraint for $[x_5,\ x_6,\ x_{10}]$ only applies to non-retrograde working fluids, so that turbine condensation and blade erosion are acceptably small, based on typical values. The constraint on P_4 enforces that the heat exchanger is strictly under positive pressure and thereby not prone to practical issues associated with maintaining a vacuum (DiPippo, 2016, p. 155).

3.3 Method

Gradient ascent is used to find a set of independent parameters that corresponds to a local maximum in η_{II}, as follows:

1. Define a vector of initial (i.e. guess) values for the independent parameters $[T_1,\ T_4,\ m_{LP}]$.
2. Define step sizes of $dT = 1$ °C and $dm = 0.01$, or 1%.
3. Generate a set of candidate vectors by perturbing each vector element by multiples of [-1,0,1] and the appropriate step size.[4]
4. Assess the value of η_{II} for each candidate vector according to Section 2.
5. Discard any candidate vectors that violate the constraints.
6. Update $[T_1,\ T_4,\ m_{LP}]$ to the candidate vector with the highest value of η_{II}.
7. Repeat back to Step #3 until no further improvement in η_{II} can be achieved.

In general, η_{II} is not strictly convex, so a converged set of independent parameters $[T_1,\ T_4,\ m_{LP}]$ represents a local maximum rather than a global maximum, and the converged result has some sensitivity to the initial conditions. For this reason, it is advisable to use heuristic methods for estimating the initial conditions, and to assess the robustness of the solution to perturbation of the initial conditions.

[4] Since optimization is three-dimensional, and each element has three degrees of freedom (decrease, remain, or increase), each iteration yields a maximum of $3^3 = 27$ valid candidate vectors.

4. TYPICAL ORC PLANT

This section considers a typical binary plant using the methods described in Sections 2 and 3 (Zarrouk and Moon, 2014, Table 6). The most common ORC working fluids are considered, along with water, in single-, double-, and triple-pressure saturated cycles. Results are shown in Table 1 below.

Table 1: Optimized utilization η_{II} as a function of the working fluid composition and number of cycle stages for $T_a = 150$ °C, $x_a = 0$, representative of a typical ORC plant. The best-performing working fluid is highlighted.

Cycle Stages	Isobutane $T_{crit} = 134.6$ °C	Butane $T_{crit} = 151.9$ °C	Isopentane $T_{crit} = 187.2$ °C	Pentane $T_{crit} = 196.5$ °C	Cyclopentane $T_{crit} = 238.5$ °C	Water $T_{crit} = 373.9$ °C
Single	0.479	0.448	0.431	0.430	0.411	0.358
Double	0.562	0.532	0.520	0.521	0.510	0.403
Triple	0.589	0.586	0.572	0.569	0.564	0.431

These results show that isobutane marginally outperforms all other working fluids considered for the assumed production conditions. A double-pressure cycle appears most appropriate, as introducing a third cycle stage increases the utilization η_{II} by less than 5%, which might not justify the additional cost and complexity. These diminishing returns corroborate the observation that single- and double-pressure plants are the most common form of ORCs. Examples of geothermal plants that have historically used isobutane include Salt Wells, Magmamax, Raft River, and Heber (DiPippo, 2016). T-s and T-q diagrams for this cycle are shown in Figure 4 below.

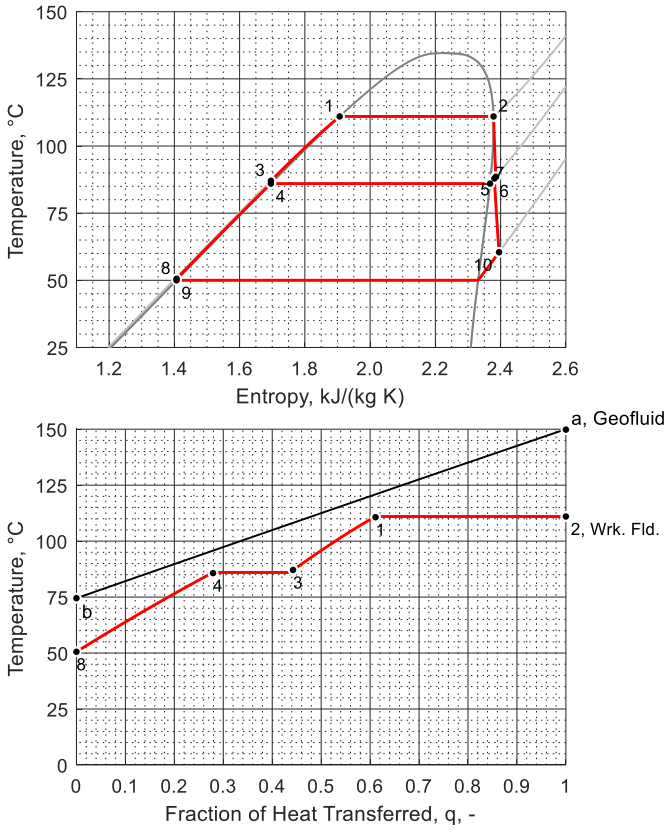


```
fluid   isobutan
q_in        354.1  kJ/kg
q_out       319.8  kJ/kg
w_net        34.3  kJ/kg
η_I         0.097  ~
x_min       1.000  ~
```

	T	P	h	s	x	m	ρ
1	111.0	24.27	503.1	1.91	0.000	0.760	401.3
2	111.0	24.27	684.3	2.38	1.000	0.760	74.3
3	87.0	24.27	424.6	1.70	NaN	0.760	462.7
4	86.0	15.19	422.6	1.70	0.000	1.000	458.8
5	88.5	15.19	670.2	2.39	1.000	0.760	40.2
6	87.9	15.19	668.7	2.38	NaN	1.000	40.4
7	86.0	15.19	663.8	2.37	1.000	0.240	41.0
8	50.6	15.19	323.8	1.41	NaN	1.000	519.1
9	50.0	6.86	322.2	1.41	0.000	1.000	517.3
10	60.4	6.86	642.0	2.40	1.000	1.000	16.7

Geofluid

Nominal Pressure	4.8	bar
Inlet Temperature	150.0	°C
Inlet Enthalpy	632.4	kJ/kg
Outlet Temperature	74.5	°C
Outlet Enthalpy	312.5	kJ/kg
Mass Flow Rate	806.9	kg/s

Plant

Mass Flow Rate (Wrk. Fld.)	729.1	kg/s
Turbine Stages	3	~
Last-Stage Blade Length	5.7	inch
Overall Turbine Diameter	0.8	m
Heat Input	258.1	MWt
Condenser Rejection	233.1	MWt
Gross Output	25.0	MWe
Utilization, η_II	0.562	~

Figure 4: Optimized double-pressure saturated isobutane plant for $T_a = 150$ °C and $x_a = 0$.

The cycles are well matched, which can be seen from their similar shapes in T-q coordinates, the equalization of the two pinch points at States 4 and 1, both with $\Delta T \approx 10$ °C, and the appropriately low geofluid outlet temperature T_b. Although superheating at State 2 improves the T-q curve match and q_{in}, it more significantly increases q_{out}, and thereby the net effect on utilization η_{II} is adverse. For this reason, retrograde fluids (i.e. ORCs) do not typically benefit from superheated or supercritical cycles, and instead favor saturated cycles.

5. WORKING FLUID SELECTION

The exercise of selecting the working fluid that maximizes utilization η_{II} can be generalized as a function of the source temperature T_a and quality x_a. Shown in Figures 5 and 6 below are the specific cases of saturated liquid with $x_a = 0$, and saturated vapor with $x_a = 1$, again using the methods described in Sections 2 and 3.

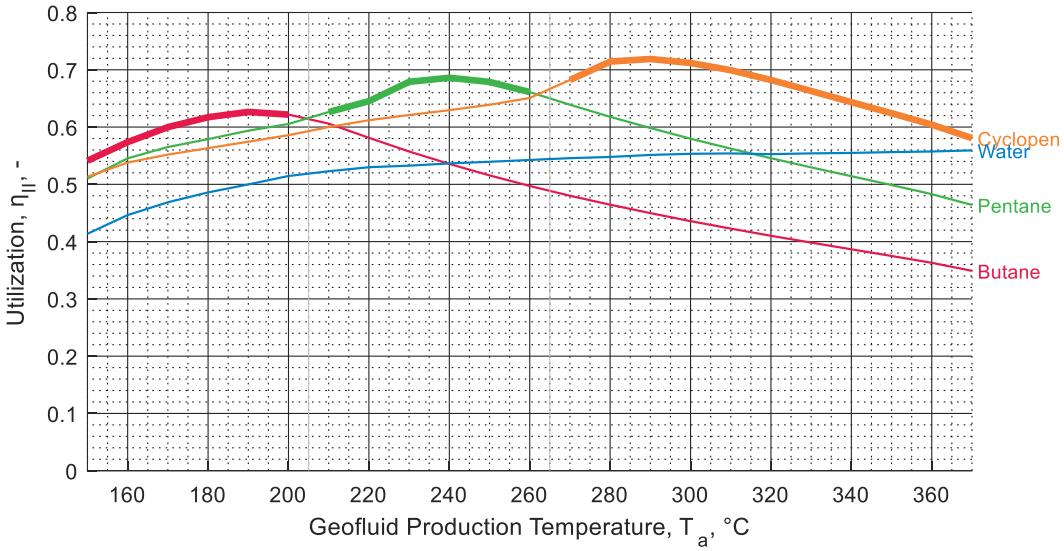

Figure 5: Ideal utilization η_{II} versus working fluid and source temperature T_a for $x_a = 0$ with double-pressure saturated cycles. Each working fluid is bolded over the temperature range where it exhibits superior utilization, where applicable.

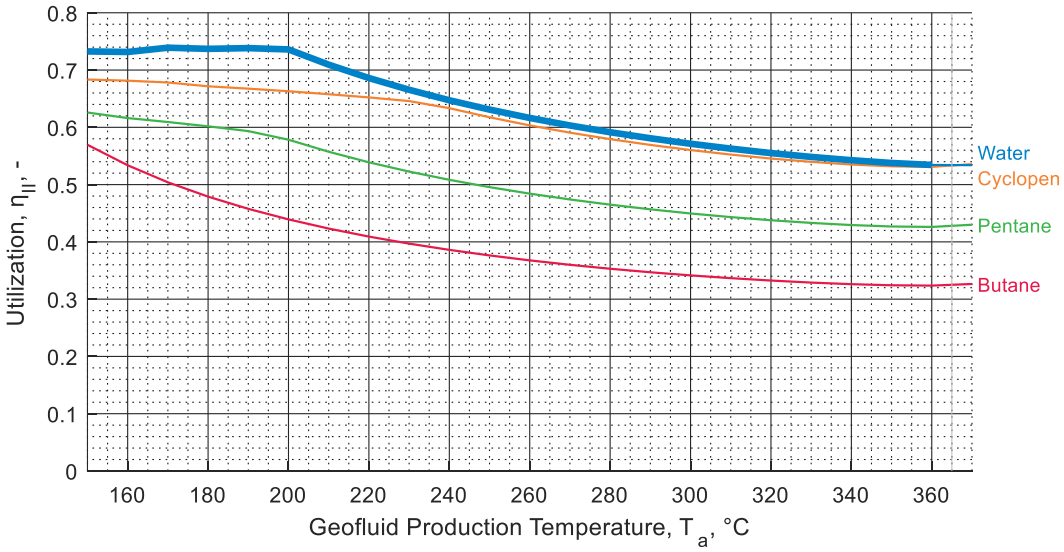

Figure 6: Ideal utilization η_{II} versus working fluid and source temperature T_a for $x_a = 1$ with double-pressure saturated cycles. Each working fluid is bolded over the temperature range where it exhibits superior utilization, where applicable.

These figures show that when $x_a = 0$, i.e. geofluid production is liquid-dominated, higher production temperatures T_a favor the use of working fluids with higher critical temperatures T_{crit}; that is, the two temperatures are correlated. Water outperforms butane and pentane, the most common ORC working fluids, above about 300 °C, although cyclopentane offers still higher utilization above about 250 °C, as corroborated in Zia et al. (2013, p. 13). However, as $x_a \to 1$ and production becomes more vapor-dominated, the advantage shifts in favor of water, independent of the production temperature T_a.

Additional factors involved in selecting a working fluid include cost, safety, and scalability. ORC units are most cost-effective at small scale, with fielded units not currently exceeding 10-25 MWe (Macchi and Astolfi, 2017, p. 3; Martinez, 2024). This is in part because the various working fluids required range in cost from around 10-50 $/gal.[5] At this smaller scale, only a relatively modest working fluid inventory is required, typically around 2,500 gal/MWe, constituting less than 10% of the total plant cost. However, research indicates that

[5] Per Macchi and Astolfi, 2017, p. 180, adjusted for inflation, with a nominal fluid density of 600 kg/m^3.

a single geothermal well producing at $T_a > 300$ °C could produce over 30 MWe, exceeding the capacity of an ORC unit (Hjartarson et al., 2014; Dichter, 2024). Although ORC hydrocarbons have a low global warming potential (GWP) and ozone depletion potential (ODP), they are nonetheless both toxic and flammable (DiPippo, 2016, p. 207). Their use therefore requires special safety equipment, authorizations, and operating procedures. For these reasons, they are disadvantaged in terms of social acceptance, and siting large-scale projects in certain jurisdictions may be prohibitively difficult – for example, in the European Union, because of the Seveso Directives that regulate the industrial use of hazardous substances (Macchi and Astolfi, 2017, p. 181). In comparison, water is typically less than 0.01 $/gal, and is trivially non-toxic and non-flammable. Further, steam turbines are currently manufactured with capacities ranging from around 10 MWe to 2 GWe, better matching the output potential of geothermal wells with $T_a > 300$ °C (Siemens Energy, 2021; DiPippo, 2016, p. 356).

In summary, water and cyclopentane offer competitive utilization as binary cycle working fluids where $T_a > 300$ °C. In the following section, the performance of these two working fluids is compared in greater detail.

6. HIGH-TEMPERATURE PLANTS

For the sake of comparison, the production temperature is taken as $T_a = 350$ °C, and the cases of saturated liquid with $x_a = 0$, saturated vapor with $x_a = 1$, and superheated vapor with $P_a = 50$ bar are considered. Per Figures 5 and 6, the working fluids considered are water and cyclopentane, with the latter representing ORCs.

Figures 7-9 on the following pages show examples of high-temperature binary plants that were designed based on the methods described in Sections 2 and 3. These show that water confers more flexibility in the working fluid cycle design, as multiple cycle stages and superheating can be used to more effectively transfer heat between the two fluids. This can be attributed to its non-retrograde condensation, and relatively high critical temperature of $T_{crit} = 373.9$ °C. In contrast, cyclopentane has retrograde condensation and a lower $T_{crit} = 238.5$ °C, and thereby benefits from neither of these cycle design strategies, as described in Section 4.

Table 2 below summarizes key performance metrics for the plants shown in Figures 7-9. Cyclopentane indeed confers a more compact turbine, primarily in the sense of the last-stage blade length r_{blade}. However, the quantity of stages n and overall diameter are both fairly similar to that of a steam turbine, and the disparity decreases as h_a increases. This can be attributed to cyclopentane's greater compressibility as compared to more common ORC working fluids, which require significantly fewer turbine stages as shown in Figure 4. All values for r_{blade} and n are feasibly within current limits, as described in Section 2.4.

However, the turbine represents a relatively small fraction of a binary plant's overall cost, which in practice is dominated by other components including the wells, heat exchanger, and condenser. These latter costs can be estimated as being proportional to the required geofluid production rate $\dot{m}_g$, heat transfer rate $\dot{Q}_h$, and heat rejection rate $\dot{Q}_c$ respectively. Secondary factors that favor the use of water over an ORC include the cost of the working fluid inventory, as described in Section 5, and the cost of the process piping, which may be correlated with the working fluid mass flow rate $\dot{m}_w$. Overall, this comparison favors the use of water over an ORC for $T_a \approx 350$ °C.

Table 2: Comparison of binary plants at 25 MWe scale, as a function of production phase and working fluid. Cases are in order of increasing production enthalpy h_a. Highlighting denotes which of the two working fluids has more favorable performance.

Component	Quantity	Symbol	Units	Saturated Liquid $x_a = 0$		Saturated Vapor $x_a = 1$		Superheated Vapor $P_a = 50$ bar	
Working Fluid	Composition	-	-	Cyclopen.	Water	Cyclopen.	Water	Cyclopen.	Water
	Mass Flow Rate	$\dot{m}_w$	kg/s	206.1	40.8	206.1	32.9	206.1	32.6
Geofluid	Mass Flow Rate	$\dot{m}_g$	kg/s	85.7	88.2	52.4	41.4	42.8	33.2
Turbine	Stage Quantity	n	-	6	7	6	8	6	8
	Last-Stage Blade Len.	r_{blade}	inch	9.1	19.2	9.1	16.4	9.1	16.4
	Overall Diameter	-	m	1.0	1.5	1.0	1.3	1.0	1.3
Heat Exch.	Heat Transfer Rate	$\dot{Q}_h$	MWt	120.1	112.0	120.1	92.3	120.1	92.6
Condenser	Heat Rejection Rate	$\dot{Q}_c$	MWt	95.1	87.0	95.1	67.3	95.1	67.6
Plant	Thermal Efficiency	η_I	-	0.208	0.223	0.208	0.271	0.208	0.270
	Utilization	η_{II}	-	0.623	0.606	0.532	0.673	0.583	0.752

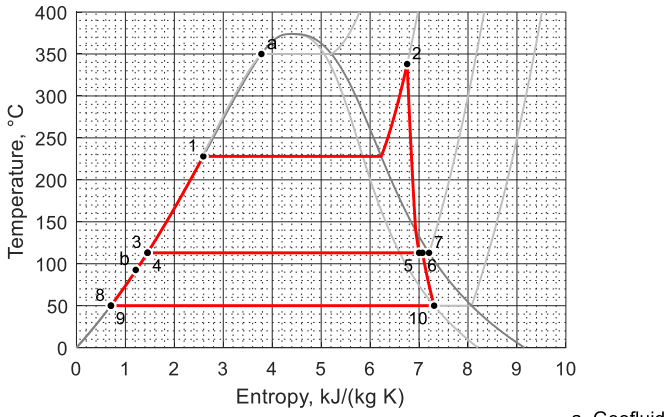

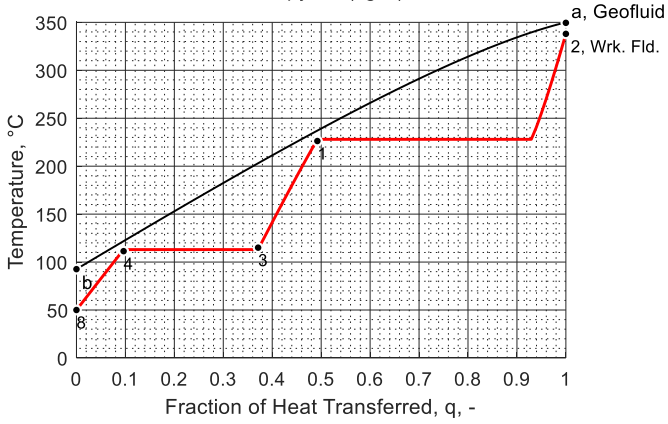

fluid	water
q_in	2747.7 kJ/kg
q_out	2134.3 kJ/kg
w_net	613.3 kJ/kg
η_I	0.223 ~
x_min	0.896 ~

	T	P	h	s	x	m	ρ
1	228.0	26.99	981.0	2.59	0.000	0.660	829.7
2	338.0	26.99	3094.9	6.76	NaN	0.660	10.1
3	113.2	26.99	477.0	1.45	NaN	0.660	949.7
4	113.0	1.59	474.3	1.45	0.000	1.000	948.6
5	113.0	1.59	2617.3	7.00	0.965	0.660	0.9
6	113.0	1.59	2643.9	7.07	0.977	1.000	0.9
7	113.0	1.59	2695.7	7.20	1.000	0.340	0.9
8	50.0	1.59	209.7	0.70	NaN	1.000	988.0
9	50.0	0.12	209.6	0.70	0.000	1.000	988.0
10	50.0	0.12	2343.9	7.31	0.896	1.000	0.1

Geofluid

Nominal Pressure	165.4	bar
Inlet Temperature	350.0	°C
Inlet Enthalpy	1671.3	kJ/kg
Outlet Temperature	92.6	°C
Outlet Enthalpy	400.9	kJ/kg
Mass Flow Rate	88.2	kg/s

Plant

Mass Flow Rate (Wrk. Fld.)	40.8	kg/s
Turbine Stages	7	~
Last-Stage Blade Length	19.2	inch
Overall Turbine Diameter	1.5	m
Heat Input	112.0	MWt
Condenser Rejection	87.0	MWt
Gross Output	25.0	MWe
Utilization, η_II	0.606	~

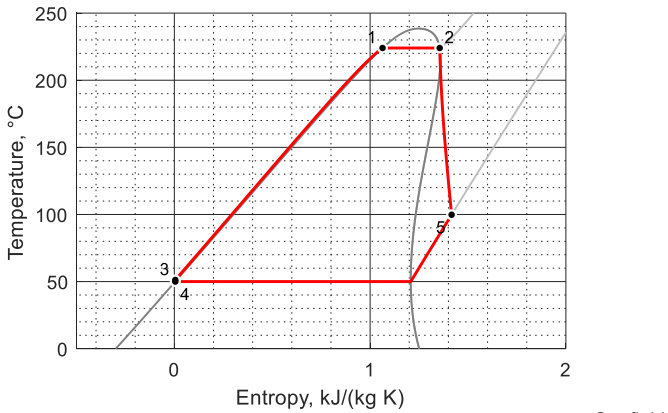

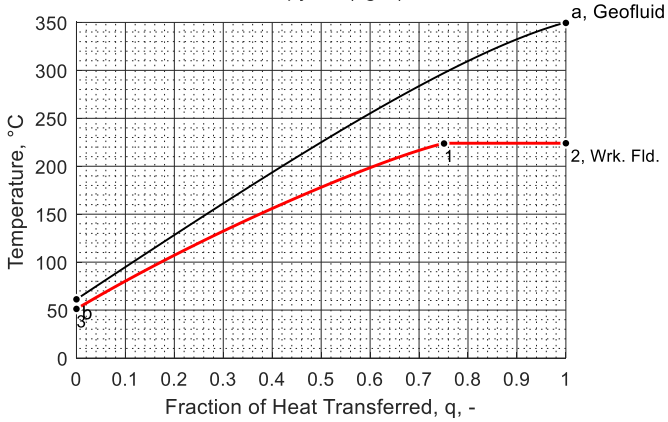

fluid	cyclopen
q_in	582.8 kJ/kg
q_out	461.4 kJ/kg
w_net	121.3 kJ/kg
η_I	0.208 ~
x_min	1.000 ~

	T	P	h	s	x	m	ρ
1	224.0	37.40	444.3	1.06	0.000	1.000	434.0
2	224.0	37.40	589.4	1.36	1.000	1.000	126.7
3	51.2	37.40	6.6	0.00	NaN	1.000	718.1
4	50.0	1.04	1.6	0.00	0.000	1.000	715.0
5	99.8	1.04	463.0	1.42	1.000	1.000	2.4

Geofluid

Nominal Pressure	165.4	bar
Inlet Temperature	350.0	°C
Inlet Enthalpy	1671.3	kJ/kg
Outlet Temperature	61.2	°C
Outlet Enthalpy	270.3	kJ/kg
Mass Flow Rate	85.7	kg/s

Plant

Mass Flow Rate (Wrk. Fld.)	206.1	kg/s
Turbine Stages	6	~
Last-Stage Blade Length	9.1	inch
Overall Turbine Diameter	1.0	m
Heat Input	120.1	MWt
Condenser Rejection	95.1	MWt
Gross Output	25.0	MWe
Utilization, η_II	0.623	~

Figure 7: Comparison of 350 °C saturated liquid production with water (top) and cyclopentane (bottom) as working fluids.

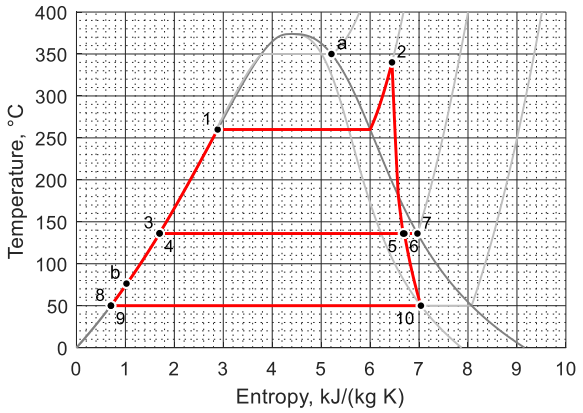

fluid	water
q_in	2807.4 kJ/kg
q_out	2047.1 kJ/kg
w_net	760.3 kJ/kg
η_I	0.271 ~
x_min	0.859 ~

	T	P	h	s	x	m	ρ
1	260.0	46.96	1135.2	2.89	0.000	0.910	783.5
2	340.0	46.96	3050.5	6.45	NaN	0.910	18.4
3	136.4	46.96	576.9	1.70	NaN	0.910	931.6
4	136.0	3.23	572.2	1.70	0.000	1.000	929.6
5	136.0	3.23	2608.5	6.67	0.944	0.910	1.9
6	136.0	3.23	2619.3	6.70	0.949	1.000	1.9
7	136.0	3.23	2728.3	6.97	1.000	0.090	1.8
8	50.0	3.23	209.9	0.70	NaN	1.000	988.1
9	50.0	0.12	209.6	0.70	0.000	1.000	988.0
10	50.0	0.12	2256.6	7.04	0.859	1.000	0.1

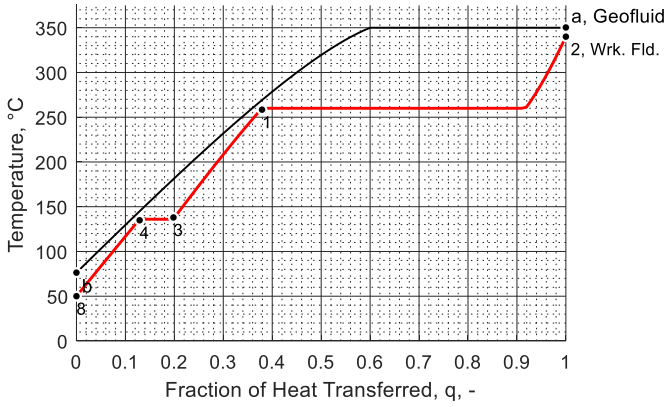

Geofluid

Nominal Pressure	165.4	bar
Inlet Temperature	350.0	°C
Inlet Enthalpy	2563.3	kJ/kg
Outlet Temperature	76.3	°C
Outlet Enthalpy	333.1	kJ/kg
Mass Flow Rate	41.4	kg/s

Plant

Mass Flow Rate (Wrk. Fld.)	32.9	kg/s
Turbine Stages	8	~
Last-Stage Blade Length	16.4	inch
Overall Turbine Diameter	1.3	m
Heat Input	92.3	MWt
Condenser Rejection	67.3	MWt
Gross Output	25.0	MWe
Utilization, η_II	0.673	~

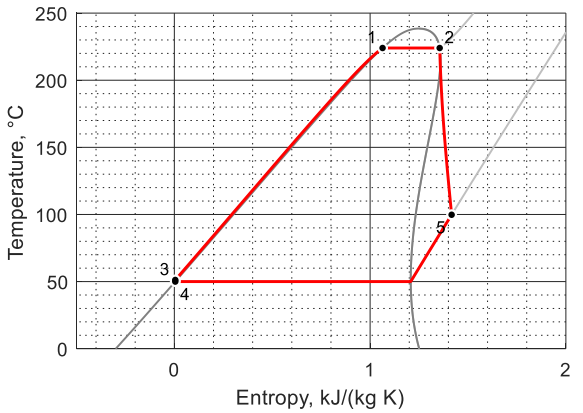

fluid	cyclopen
q_in	582.8 kJ/kg
q_out	461.4 kJ/kg
w_net	121.3 kJ/kg
η_I	0.208 ~
x_min	1.000 ~

	T	P	h	s	x	m	ρ
1	224.0	37.40	444.3	1.06	0.000	1.000	434.0
2	224.0	37.40	589.4	1.36	1.000	1.000	126.7
3	51.2	37.40	6.6	0.00	NaN	1.000	718.1
4	50.0	1.04	1.6	0.00	0.000	1.000	715.0
5	99.8	1.04	463.0	1.42	1.000	1.000	2.4

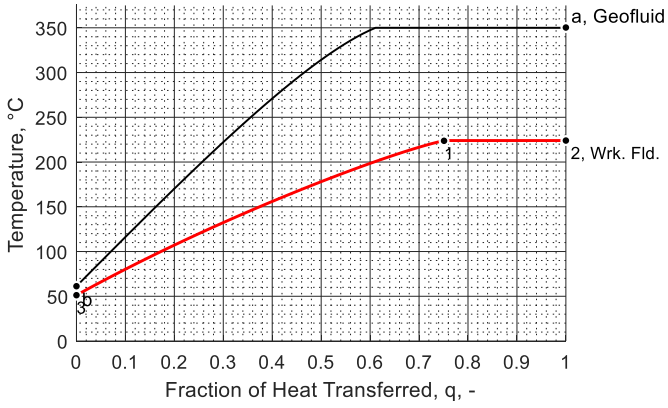

Geofluid

Nominal Pressure	165.4	bar
Inlet Temperature	350.0	°C
Inlet Enthalpy	2563.3	kJ/kg
Outlet Temperature	61.2	°C
Outlet Enthalpy	270.4	kJ/kg
Mass Flow Rate	52.4	kg/s

Plant

Mass Flow Rate (Wrk. Fld.)	206.1	kg/s
Turbine Stages	6	~
Last-Stage Blade Length	9.1	inch
Overall Turbine Diameter	1.0	m
Heat Input	120.1	MWt
Condenser Rejection	95.1	MWt
Gross Output	25.0	MWe
Utilization, η_II	0.532	~

Figure 8: Comparison of 350 °C saturated vapor production with water (top) and cyclopentane (bottom) as working fluids.

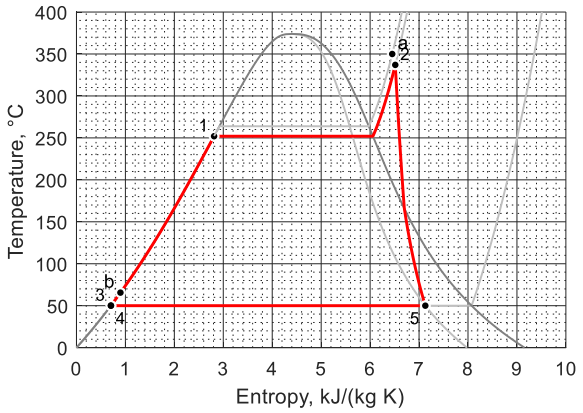

fluid	water
q_in	2844.0 kJ/kg
q_out	2076.2 kJ/kg
w_net	767.8 kJ/kg
η_I	0.270 ~
x_min	0.872 ~

	T	P	h	s	x	m	ρ
1	252.0	41.16	1095.8	2.81	0.000	1.000	795.8
2	337.0	41.16	3057.7	6.51	NaN	1.000	16.0
3	50.1	41.16	213.7	0.70	NaN	1.000	989.7
4	50.0	0.12	209.6	0.70	0.000	1.000	988.0
5	50.0	0.12	2285.7	7.13	0.872	1.000	0.1

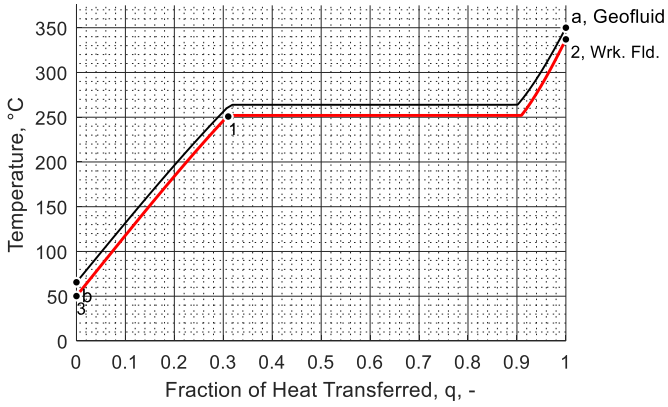

Geofluid

Nominal Pressure	50.0	bar
Inlet Temperature	350.0	°C
Inlet Enthalpy	3069.4	kJ/kg
Outlet Temperature	65.6	°C
Outlet Enthalpy	278.8	kJ/kg
Mass Flow Rate	33.2	kg/s

Plant

Mass Flow Rate (Wrk. Fld.)	32.6	kg/s
Turbine Stages	8	~
Last-Stage Blade Length	16.4	inch
Overall Turbine Diameter	1.3	m
Heat Input	92.6	MWt
Condenser Rejection	67.6	MWt
Gross Output	25.0	MWe
Utilization, η_II	0.752	~

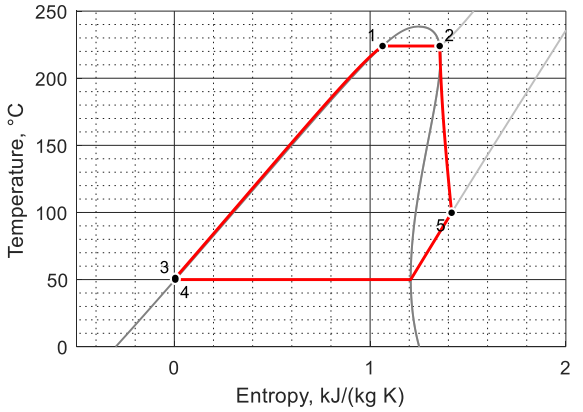

fluid	cyclopen
q_in	582.8 kJ/kg
q_out	461.4 kJ/kg
w_net	121.3 kJ/kg
η_I	0.208 ~
x_min	1.000 ~

	T	P	h	s	x	m	ρ
1	224.0	37.40	444.3	1.06	0.000	1.000	434.0
2	224.0	37.40	589.4	1.36	1.000	1.000	126.7
3	51.2	37.40	6.6	0.00	NaN	1.000	718.1
4	50.0	1.04	1.6	0.00	0.000	1.000	715.0
5	99.8	1.04	463.0	1.42	1.000	1.000	2.4

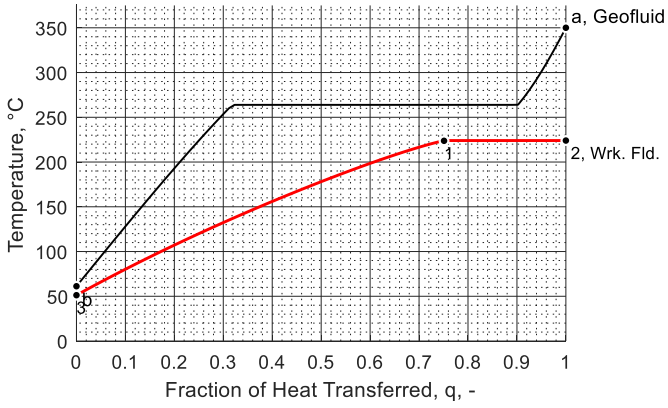

Geofluid

Nominal Pressure	50.0	bar
Inlet Temperature	350.0	°C
Inlet Enthalpy	3069.4	kJ/kg
Outlet Temperature	61.2	°C
Outlet Enthalpy	260.6	kJ/kg
Mass Flow Rate	42.8	kg/s

Plant

Mass Flow Rate (Wrk. Fld.)	206.1	kg/s
Turbine Stages	6	~
Last-Stage Blade Length	9.1	inch
Overall Turbine Diameter	1.0	m
Heat Input	120.1	MWt
Condenser Rejection	95.1	MWt
Gross Output	25.0	MWe
Utilization, η_II	0.583	~

Figure 9: Comparison of 350 °C superheated vapor production with water (top) and cyclopentane (bottom) as working fluids.

7. CONCLUSION

This paper demonstrated the advantages of using water as a binary cycle working fluid for geothermal production at around 300-350 °C, as compared to organic Rankine cycles (ORCs). A model of an ideal double-pressure saturated binary plant was developed, focusing on the performance of the heat exchanger, turbine, and condenser. It was noted that this model could be generalized to single- and triple-pressure cycles, as well as superheated cycles. Particular attention was given to the physical sizing of the turbine, in the sense of its number of stages, and last-stage blade length. It was shown that only two unique optimization criteria exist: thermal efficiency, and utilization (or exergetic efficiency), with the latter being preferable for heat engines generally, and binary plants specifically. A method of constrained gradient ascent was developed for determining the approximate cycle parameters that maximize utilization; the limitations of this method associated with local optima were also discussed.

This methodology was then applied to a scenario representative of a typical binary plant: production of 150 °C saturated liquid geofluid. It was found that a double-pressure saturated ORC conferred superior utilization with an appropriate level of plant complexity, with isobutane outperforming other hydrocarbons and water. Effective cycle optimization was verified from curve matching of the two cycles in T-q (temperature-heat transfer) coordinates, pinch point equalization, and an appropriately low geofluid outlet temperature.

The exercise of optimal working fluid selection was then generalized to higher geofluid production temperatures. This showed that for liquid-phase production, higher geofluid production temperatures favor the use of working fluids with higher critical temperatures. For vapor-phase production, no such dependence exists, and water outperforms ORCs under essentially all conditions. Overall, it was found that water offers favorable working fluid performance as geofluid production exceeds about 300 °C and/or becomes increasingly vapor-dominated. Practical aspects of cost, safety, and scalability were also discussed, favoring water over ORCs.

Finally, a series of high-temperature geothermal binary plants were considered. These were assumed to have a fixed gross output, and a geofluid production temperature of 350 °C. Three production scenarios were considered: saturated liquid, saturated vapor, and superheated vapor, with cyclopentane (representing ORCs) and water as candidate working fluids. It was found that cyclopentane conferred a somewhat more compact turbine, although the sizing of the steam turbine was also feasibly within current limits. Otherwise, water conferred more significant advantages in the sense of more cycle design flexibility, fewer wells, a smaller heat exchanger, and a smaller condenser, because of higher thermal efficiency and utilization, ranging from about 22-27% and 61-75% respectively.

REFERENCES

Çengel, Y.A., Cimbala, J.M., and Turner, R.H.: Fundamentals of Thermal-Fluid Sciences, McGraw-Hill, 4th edition, (2012).

Curzon, F.L., and Ahlborn, B.: Efficiency of a Carnot Engine at Maximum Power Output, American Journal of Physics, (1975).

Dichter, D.: Ideal Thermal-Hydraulic Performance of Geothermal Power Systems Above 300 °C, Transactions, Geothermal Rising Conference, (2024).

DiPippo, R.: Geothermal Power Plants, Butterworth-Heinemann, 4th edition, (2016).

Hjartarson, S., et al.: Utilization of the Chloride Bearing, Superheated Steam from IDDP-1, Geothermics, (2014).

Lemmon, E.W., et al.: NIST Standard Reference Database 23: Reference Fluid Thermodynamic and Transport Properties-REFPROP, Version 10.0, National Institute of Standards and Technology, (2018).

Li, K.W., and Priddy, A.P.: Power Plant Systems Design, John Wiley & Sons, (1982).

Macchi, E., and Astolfi, M.: Organic Rankine Cycle (ORC) Power Systems, Woodhead Publishing, 1st edition, (2017).

Martinez, M.: Ormat: Renewing Earth's Energy Future, Proceedings, Geothermal Energy Machinery and Systems (GEMS) Workshop, Southwest Research Institute, (2024).

Ormat Technologies, Inc.: Plain Bearings Turbine – Revolutionizing Geothermal Energy, Article, Accessed Jan 10 2025, (2024).

Milora, S., and Tester, J.: Geothermal Energy as a Source of Electric Power, MIT Press, (1976).

Reitlinger, H.B.: Sur L'Utilisation de la Chaleur Dans Les Machines À Feu, Vaillant-Carmanne, Liège, (1929).

Siemens Energy: Utility Steam Turbines from 90 to 1,900 MW, Brochure, Accessed Jan 9 2025, (2021).

Tabor, H.Z., and Bronicki, L.: Vapor Turbines, U.S. Patent 3,040,528, (1962).

Zarrouk, S., and Moon, H.: Efficiency of Geothermal Power Plants: A Worldwide Review, Geothermics, (2014).

Zia, J., et al.: High-Potential Working Fluids for Next Generation Binary Cycle Geothermal Power Plants, Phase 3 & Final Report, U.S. Department of Energy, (2013).